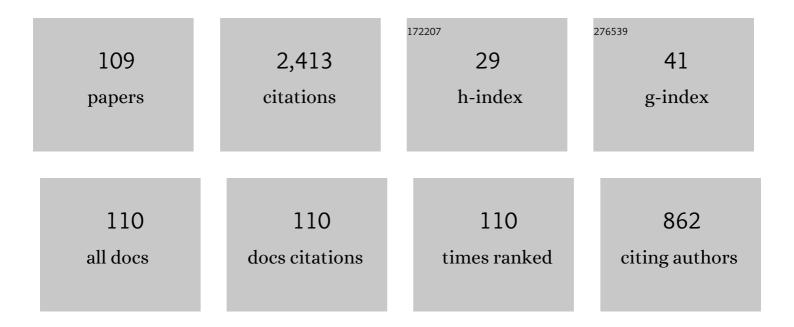
List of Publications by Year in descending order

Source: https://exaly.com/author-pdf/1614085/publications.pdf Version: 2024-02-01



#	Article	IF	CITATIONS
1	Forming limit diagrams and mechanical properties of AA1050/Ti CP2 multilayered composite produced by the accumulative roll bonding technique. Proceedings of the Institution of Mechanical Engineers, Part B: Journal of Engineering Manufacture, 2023, 237, 643-653.	1.5	1
2	Formability and fractography of AA5754/polyethylene/AA5754 sandwich composites. Mechanics Based Design of Structures and Machines, 2022, 50, 1253-1267.	3.4	8
3	Effect of annealing on formability and mechanical properties of AA1050/Mg-AZ31B bilayer sheets fabricated by explosive welding method. International Journal of Advanced Manufacturing Technology, 2022, 118, 775-784.	1.5	12
4	Finite Element Simulation of the Parallel Tubular Channel Angular Pressing Process for Al–Cu Bimetallic Tube with Experimental Verification. Transactions of the Indian Institute of Metals, 2022, 75, 91-100.	0.7	4
5	Finite element simulations and experimental verifications for forming limit curve determination of two-layer aluminum/brass sheets considering the incremental forming process. Proceedings of the Institution of Mechanical Engineers, Part L: Journal of Materials: Design and Applications, 2022, 236, 361-373.	0.7	3
6	An Exhaustive Evaluation of Fracture Toughness, Microstructure, and Mechanical Characteristics of Friction Stir Welded Al6061 Alloy and Parameter Model Fitting Using Response Surface Methodology. Journal of Materials Engineering and Performance, 2022, 31, 3418-3436.	1.2	9
7	A novel experimental approach in determining forming limit diagrams by considering the effect of normal pressure. International Journal of Material Forming, 2022, 15, 1.	0.9	5
8	Severe plastic deformation (SPD) of biodegradable magnesium alloys and composites: A review of developments and prospects. Journal of Magnesium and Alloys, 2022, 10, 938-955.	5.5	64
9	Study of forming limit curves and mechanical properties of three-layered brass (CuZn10)/ low carbon steel (St14) /brass (CuZn10) composite considering the effect of annealing temperature. Journal of Materials Research and Technology, 2022, 18, 4672-4682.	2.6	6
10	Review of selective laser melting of magnesium alloys: advantages, microstructure and mechanical characterizations, defects, challenges, and applications. Journal of Materials Research and Technology, 2022, 19, 1537-1562.	2.6	64
11	High cycle fatigue behavior of bimetallic Al 7025/CP-Mg rods produced by rotary swaging. Journal of Materials Research and Technology, 2022, 19, 3321-3336.	2.6	4
12	On the impacts of cutting parameters on surface roughness, tool wear mode and size in slot milling of A356 metal matrix composites reinforced with silicon carbide elements. Proceedings of the Institution of Mechanical Engineers, Part B: Journal of Engineering Manufacture, 2021, 235, 1655-1667.	1.5	10
13	Investigation of forming limit diagram and mechanical properties of the bimetallic Al/Cu composite sheet at different temperatures which fabricated by explosive welding. Proceedings of the Institution of Mechanical Engineers, Part B: Journal of Engineering Manufacture, 2021, 235, 73-84.	1.5	7
14	Investigation of forming limit curves and mechanical properties of 316 stainless steel/St37 steel tailor-welded blanks produced by tungsten inert gas and friction stir welding method. CIRP Journal of Manufacturing Science and Technology, 2021, 32, 437-446.	2.3	19
15	Manufacturing of three-layered sandwich composite of AA1050/LZ91/AA1050 using cold roll bonding process. Proceedings of the Institution of Mechanical Engineers, Part B: Journal of Engineering Manufacture, 2021, 235, 1363-1372.	1.5	10
16	The role of applied strain and volume percentage of components on mechanical properties and fracture toughness in multilayered Al/Mg composite fabricated by the accumulative roll bonding process. Materials Research Express, 2021, 8, 026508.	0.8	2
17	Evaluation of forming limit diagrams using Nakazima out-of-plane test and incremental forming process for two-phase magnesium–lithium alloy sheet. Journal of the Brazilian Society of Mechanical Sciences and Engineering, 2021, 43, 1.	0.8	0
18	A method and apparatus for determination of the ultrasonic-assisted forming limit diagram. Proceedings of the Institution of Mechanical Engineers, Part C: Journal of Mechanical Engineering Science, 2021, 235, 7062-7073.	1.1	10

RAMIN HASHEMI

#	Article	IF	CITATIONS
19	Experimental study of the defects, mechanical and microstructural characteristics of friction-stir-welded Al 6061 sheets. Surface Topography: Metrology and Properties, 2021, 9, 035012.	0.9	5
20	Formability of Tri-layered IF240/AZ31/IF240 Composite with Strong Bonding: Experimental and Finite Element Modeling. Journal of Materials Engineering and Performance, 2021, 30, 8402-8411.	1.2	2
21	An experimental investigation of mechanical properties, forming limit curves, and bending behavior of aluminum-polymer sandwich composites. Materials Research Express, 2021, 8, 086516.	0.8	1
22	Investigation of annealing treatment on the interfacial and mechanical properties of Al5052/Cu multilayered composites subjected to ARB process. Journal of Alloys and Compounds, 2021, 871, 159513.	2.8	34
23	The role of thickness on the fracture behavior of Al/Mg–Li/Al composite processed by cold roll bonding. Materials Science & Engineering A: Structural Materials: Properties, Microstructure and Processing, 2021, 824, 141851.	2.6	14
24	Effects of strain accumulation and annealing on interfacial microstructure and grain structure (Mg) Tj ETQq0 0 0 Materials Research and Technology, 2021, 14, 392-406.	rgBT /Ove 2.6	rlock 10 Tf 5 39
25	DIC-based experimental study of fracture toughness through R-curve tests in a multi-layered Al-Mg (LZ91) composite fabricated by ARB. Journal of Alloys and Compounds, 2021, 883, 160843.	2.8	24
26	Study of mechanical properties and wear resistance of Al 1050/Brass (70/30)/Al 1050 composite sheets fabricated by the accumulative roll bonding process. Journal of Manufacturing Processes, 2021, 71, 407-416.	2.8	17
27	Analytical and numerical investigation of wrinkling limit diagram in deep drawing of two-layer sheets with experimental verification. Proceedings of the Institution of Mechanical Engineers, Part L: Journal of Materials: Design and Applications, 2021, 235, 974-990.	0.7	4
28	The influence of post-annealing and ultrasonic vibration on the formability of multilayered Al5052/MgAZ31B composite. Materials Science and Technology, 2021, 37, 78-85.	0.8	31
29	Evaluation of Temperature Effects on Forming Limit Diagrams of AA6061-T6 Considering the Marciniak and Kuczynski Model. Journal of Testing and Evaluation, 2021, 49, 20190011.	0.4	3
30	Asymmetric accumulative roll bonding of aluminum/copper composite sheets. Proceedings of the Institution of Mechanical Engineers, Part L: Journal of Materials: Design and Applications, 2021, 235, 842-852.	0.7	0
31	Anisotropic Behavior of Al1050 through Accumulative Roll Bonding. Materials, 2021, 14, 6910.	1.3	2
32	Insight into the Influence of Punch Velocity and Thickness on Forming Limit Diagrams of AA 6061 Sheets—Numerical and Experimental Analyses. Metals, 2021, 11, 2010.	1.0	2
33	Finite element and experimental method for analyzing the effects of martensite morphologies on the formability of DP steels. Mechanics Based Design of Structures and Machines, 2020, 48, 525-541.	3.4	64
34	Prediction of FLD for sheet metal by considering through-thickness shear stresses. Mechanics Based Design of Structures and Machines, 2020, 48, 755-772.	3.4	71
35	The effect of temperature on the mechanical properties and forming limit diagram of aluminum strips fabricated by accumulative roll bonding process. Journal of Materials Research and Technology, 2020, 9, 1831-1846.	2.6	26
36	Experimental investigation of spring-back phenomenon through an L-die bending process for multilayered sheets produced by the accumulative press bonding technique. Proceedings of the Institution of Mechanical Engineers, Part L: Journal of Materials: Design and Applications, 2020, 234, 1550-1559.	0.7	5

#	Article	IF	CITATIONS
37	Comparison between Explosive Welding and Roll-Bonding Processes of AA1050/Mg AZ31B Bilayer Composite Sheets Considering Microstructure and Mechanical Properties. Journal of Materials Engineering and Performance, 2020, 29, 6322-6332.	1.2	16
38	Experimental and numerical assessment of energy absorption capacity of thin-walled Al 5083 tube produced by PTCAP process. Transactions of Nonferrous Metals Society of China, 2020, 30, 1238-1248.	1.7	6
39	Production of Al/Mg-Li composite by the accumulative roll bonding process. Journal of Materials Research and Technology, 2020, 9, 7880-7886.	2.6	37
40	Flexible bending of rectangular profiles: numerical and experimental investigations. Journal of Manufacturing Processes, 2020, 56, 390-399.	2.8	15
41	Experimental study of forming limit diagram and mechanical properties of aluminum foils processed by the accumulative roll bonding. Materials Research Express, 2020, 7, 126511.	0.8	8
42	Some Practical Aspects of Digital Image Correlation Technique to Evaluate Anisotropy Coefficient and Its Comparison with Traditional Method. Journal of Testing and Evaluation, 2020, 48, 4719-4734.	0.4	8
43	Influences of the constrained groove pressing on microstructural, mechanical, and fracture properties of brass sheets. Materials Research Express, 2020, 7, 116526.	0.8	9
44	Analysis of constrained groove pressing and constrained groove pressing-cross route process on AA5052 sheet for automotive body structure applications. Proceedings of the Institution of Mechanical Engineers, Part D: Journal of Automobile Engineering, 2019, 233, 1436-1452.	1.1	6
45	Influence of ARB technique on the microstructural, mechanical and fracture properties of the multilayered Al1050/Al5052 composite reinforced by SiC particles. Journal of Materials Research and Technology, 2019, 8, 4287-4301.	2.6	37
46	Ultrafine and fine particle emission in turning titanium metal matrix composite (Ti-MMC). Journal of Central South University, 2019, 26, 1563-1572.	1.2	2
47	Investigation of mechanical properties, formability, and anisotropy of dual phase Mg–7Li–1Zn. Materials Research Express, 2019, 6, 096543.	0.8	24
48	Experimental and FE analysis on spring-back of copper/aluminum layers sheet for a L-die bending process. Materials Research Express, 2019, 6, 1165h4.	0.8	11
49	Lubrication performance of rapeseed oil-based nano-lubricants in parallel tubular channel angular pressing process. Journal of Central South University, 2019, 26, 1042-1049.	1.2	4
50	Characterizing the elastic and plastic properties of the multilayered Al/Brass composite produced by ARB using DIC. Materials Science & Engineering A: Structural Materials: Properties, Microstructure and Processing, 2019, 753, 70-78.	2.6	46
51	Using digital image correlation for characterizing the elastic and plastic parameters of ultrafine-grained Al 1050 strips fabricated via accumulative roll bonding process. Materials Research Express, 2019, 6, 086542.	0.8	21
52	A comprehensive study on the effect of heat treatment on the fracture behaviors and structural properties of Mg-Li alloys using RSM. Materials Research Express, 2019, 6, 076554.	0.8	36
53	The effect of temperature on the mechanical properties and forming limit diagram of Al 5083 produced by equal channel angular rolling. International Journal of Advanced Manufacturing Technology, 2019, 105, 4389-4400.	1.5	10
54	Manufacturing of high-strength multilayered composite by accumulative roll bonding. Materials Research Express, 2019, 6, 1265e6.	0.8	17

#	Article	IF	CITATIONS
55	Evaluation of fracture toughness and rupture energy absorption capacity of as-rolled LZ71 and LZ91 Mg alloy sheet. Materials Research Express, 2019, 6, 036517.	0.8	26
56	Measurement of directional anisotropy coefficients for AA7020-T6 tubes and prediction of forming limit curve. International Journal of Advanced Manufacturing Technology, 2018, 96, 1015-1023.	1.5	15
57	Effects of normal and through-thickness shear stresses on the forming limit curves of AA3104-H19 using advanced yield criteria. International Journal of Mechanical Sciences, 2018, 137, 15-23.	3.6	20
58	Forming limit diagram of Al-Cu two-layer metallic sheets considering the Marciniak and Kuczynski theory. Proceedings of the Institution of Mechanical Engineers, Part B: Journal of Engineering Manufacture, 2018, 232, 848-854.	1.5	18
59	Forming limit diagrams of fine-grained Al 5083 produced by equal channel angular rolling process. Proceedings of the Institution of Mechanical Engineers, Part L: Journal of Materials: Design and Applications, 2018, 232, 922-930.	0.7	11
60	Forming limit diagrams by including the M–K model in finite element simulation considering the effect of bending. Proceedings of the Institution of Mechanical Engineers, Part L: Journal of Materials: Design and Applications, 2018, 232, 625-636.	0.7	45
61	Experimental investigation of mechanical properties, formability and forming limit diagrams for tailor-welded blanks produced by friction stir welding. Journal of Manufacturing Processes, 2018, 31, 310-323.	2.8	149
62	A comparative study of the extended forming limit diagrams considering strain path, through-thickness normal and shear stress. International Journal of Mechanical Sciences, 2018, 148, 316-326.	3.6	12
63	Fracture toughness investigation of Al1050/Cu/MgAZ31ZB multi-layered composite produced by accumulative roll bonding process. Materials Science & Engineering A: Structural Materials: Properties, Microstructure and Processing, 2018, 734, 427-436.	2.6	45
64	An Experimental Study of Fracture Toughness for Nano/Ultrafine Grained Al5052/Cu Multilayered Composite Processed by Accumulative Roll Bonding. Journal of Manufacturing Science and Engineering, Transactions of the ASME, 2018, 140, .	1.3	38
65	Microstructure and mechanical properties of Al/Cu/Mg laminated composite sheets produced by the ARB proces. International Journal of Minerals, Metallurgy and Materials, 2018, 25, 564-572.	2.4	61
66	Evaluation of Microstructure and Mechanical Properties of Multilayer Al5052–Cu Composite Produced by Accmulative Roll Bonding. Powder Metallurgy and Metal Ceramics, 2018, 57, 144-153.	0.4	27
67	An Experimental, Analytical, and Numerical Investigation of Hydraulic Bulge Test in Two-Layer Al–Cu Sheets. Journal of Manufacturing Science and Engineering, Transactions of the ASME, 2017, 139, .	1.3	32
68	Analysis and Simulation of Parallel Tubular Channel Angular Pressing of Al 5083 Tube. Transactions of the Indian Institute of Metals, 2017, 70, 2547-2553.	0.7	6
69	Experimental evaluation of forming limit diagram and mechanical properties of nano/ultra-fine grained aluminum strips fabricated by accumulative roll bonding. International Journal of Materials Research, 2017, 108, 1036-1044.	0.1	41
70	Experimental evaluation of the plane stress fracture toughness for ultra-fine grained aluminum specimens prepared by accumulative roll bonding process. Materials Science & Engineering A: Structural Materials: Properties, Microstructure and Processing, 2017, 708, 301-310.	2.6	58
71	Mechanical anisotropy in ultra-fine grained aluminium tubes processed by parallel-tubular-channel angular pressing. Materials Science and Technology, 2017, 33, 2265-2273.	0.8	16
72	Forming limit diagram of aluminum-copper two-layer sheets: numerical simulations and experimental verifications. International Journal of Advanced Manufacturing Technology, 2017, 90, 2713-2722.	1.5	33

#	Article	IF	CITATIONS
73	Strain measurement and determining coefficient of plastic anisotropy using digital image correlation (DIC). Mechanics and Industry, 2017, 18, 311.	0.5	11
74	Numerical and experimental study of bursting prediction in tube hydroforming of Al 7020-T6. Mechanics and Industry, 2017, 18, 411.	0.5	12
75	Forming limit curves analysis of aluminum alloy considering the through-thickness normal stress, anisotropic yield functions and strain rate. International Journal of Mechanical Sciences, 2016, 117, 93-101.	3.6	36
76	Forming limit diagram of tubular hydroformed parts considering the through-thickness compressive normal stress. Proceedings of the Institution of Mechanical Engineers, Part L: Journal of Materials: Design and Applications, 2016, 230, 332-343.	0.7	5
77	Prediction of forming limit diagrams using the modified M-K method in hydroforming of aluminum tubes. International Journal of Material Forming, 2016, 9, 297-303.	0.9	14
78	Enhancing the Mechanical Properties and Formability of Low Carbon Steel with Dual-Phase Microstructures. Journal of Materials Engineering and Performance, 2016, 25, 382-389.	1.2	98
79	Determination of forming limit curve in two-layer metallic sheets using the finite element simulation. Proceedings of the Institution of Mechanical Engineers, Part L: Journal of Materials: Design and Applications, 2016, 230, 1018-1029.	0.7	9
80	Experimental and theoretical investigation of strain path change effect on forming limit diagram of AA5083. International Journal of Advanced Manufacturing Technology, 2015, 76, 1343-1352.	1.5	23
81	Experimental studying of the effect of active area on the performance of passive direct methanol fuel cell. Ionics, 2015, 21, 2851-2862.	1.2	12
82	A methodology for determination of extended strain-based forming limit curve considering the effects of strain path and normal stress. Proceedings of the Institution of Mechanical Engineers, Part C: Journal of Mechanical Engineering Science, 2015, 229, 1537-1547.	1.1	9
83	Numerical and experimental study of formability in deep drawing of two-layer metallic sheets. International Journal of Advanced Manufacturing Technology, 2015, 80, 113-121.	1.5	32
84	Evaluation of the microstructure and mechanical properties of the ultrafine grained thin-walled tubes processed by severe plastic deformation. Metals and Materials International, 2015, 21, 1068-1073.	1.8	20
85	A different approach to estimate the process parameters in tube hydroforming. International Journal of Material Forming, 2015, 8, 355-366.	0.9	4
86	Analysis of necking in tube hydroforming by means of extended forming limit stress diagram. Engineering Solid Mechanics, 2014, 2, 73-82.	0.6	4
87	Analysis of the extended stress-based forming limit curve considering the effects of strain path and through-thickness normal stress. Materials & Design, 2014, 54, 670-677.	5.1	35
88	A simulation-based approach to the determination of forming limit diagrams. Proceedings of the Institution of Mechanical Engineers, Part B: Journal of Engineering Manufacture, 2014, 228, 1582-1591.	1.5	19
89	A Novel Approach to the Determination of Forming Limit Diagrams for Tailor-Welded Blanks. Journal of Materials Engineering and Performance, 2013, 22, 3210-3221.	1.2	26
90	The strain gradient approach to predict necking in tube hydroforming. Journal of Manufacturing Processes, 2013, 15, 51-55.	2.8	28

#	Article	IF	CITATIONS
91	The Effect of the Imposed Boundary Rate on the Formability of Strain Rate Sensitive Sheets Using the M-K Method. Journal of Materials Engineering and Performance, 2013, 22, 2522-2527.	1.2	14
92	An Incrementally Coupled Thermo-Electro-Mechanical Model for Resistance Spot Welding. Materials and Manufacturing Processes, 2012, 27, 1442-1449.	2.7	20
93	Application of the hydroforming strain- and stress-limit diagrams to predict necking in metal bellows forming process. International Journal of Advanced Manufacturing Technology, 2010, 46, 551-561.	1.5	33
94	Using the finite element method for achieving an extra high limiting drawing ratio (LDR) of 9 for cylindrical components. CIRP Journal of Manufacturing Science and Technology, 2010, 3, 262-267.	2.3	17
95	Hydroforming Limits in Metal Bellows Forming Process. Materials and Manufacturing Processes, 2010, 25, 1413-1417.	2.7	33
96	Forming limit diagrams with the existence of through-thickness normal stress. Computational Materials Science, 2010, 48, 504-508.	1.4	75
97	New formulation for vibration analysis of Timoshenko beam with double-sided cracks. Structural Engineering and Mechanics, 2010, 34, 475-490.	1.0	2
98	An improved strain gradient approach for determination of deformation localization and forming limit diagrams. Journal of Materials Processing Technology, 2009, 209, 1758-1769.	3.1	18
99	Some numerical aspects of necking solution in prediction of sheet metal forming limits by strain gradient plasticity. Materials & Design, 2009, 30, 727-740.	5.1	23
100	Implementation of the forming limit stress diagram to obtain suitable load path in tube hydroforming considering M–K model. Materials & Design, 2009, 30, 3545-3553.	5.1	55
101	A methodology for prediction of forming limit stress diagrams considering the strain path effect. Computational Materials Science, 2009, 45, 195-204.	1.4	67
102	Finding the optimum Hill index in the determination of the forming limit diagram. Proceedings of the Institution of Mechanical Engineers, Part B: Journal of Engineering Manufacture, 2009, 223, 943-944.	1.5	0
103	The strain gradient approach for determination of forming limit stress and strain diagrams. Proceedings of the Institution of Mechanical Engineers, Part B: Journal of Engineering Manufacture, 2008, 222, 467-483.	1.5	23
104	Computation of stress intensity factors (KI, KII) and T-stress for cracks reinforced by composite patching. Composite Structures, 2007, 78, 602-609.	3.1	32
105	Mixed mode fracture in an inclined center crack repaired by composite patching. Composite Structures, 2007, 81, 264-273.	3.1	33
106	The Effect of Hygrothermal Composite Patch on the Fracture of Reinforced Crack under Mixed-Mode Loading. Applied Mechanics and Materials, 2006, 5-6, 189-196.	0.2	0
107	An Analytical Approach in Prediction of Necking and Suitable Load Path in Tube Hydroforming by Using the Strain Gradient. , 0, , .		0
108	Forming Limit Diagrams of Ground St14 Steel Sheets with Different Thicknesses. SAE International Journal of Materials and Manufacturing, 0, 5, 60-64.	0.3	22

#	Article	IF	CITATIONS
109	Investigation of Mechanical Properties, Formability, and Anisotropy of Dual Phase Mg-7Li-1Zn. SSRN Electronic Journal, 0, , .	0.4	1